UNIVERSITY *of York*

This is a repository copy of *Selective C-H Activation at a Molecular Rhodium Sigma-Alkane Complex by Solid/Gas Single-Crystal to Single-Crystal H/D Exchange*.

JACS

Article

Selective C−H Activation at a Molecular Rhodium Sigma-Alkane Complex by Solid/Gas Single-Crystal to Single-Crystal H/D Exchange

F. Mark Chadwick,[†,⊥] Tobias Krämer,[‡,⊥] Torsten Gutmann,[§] Nicholas H. Rees,[†] Amber L. Thompson,[†] Alison J. Edwards,[∥] Gerd Buntkowsky,[§] Stuart A. Macgregor,*[‡] and Andrew S. Weller*[†]

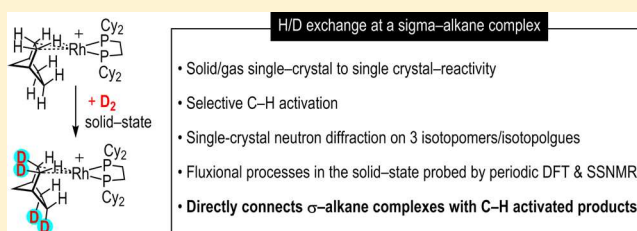[†]Department of Chemistry, Mansfield Road, University of Oxford, Oxford OX1 3TA, U.K.

[‡]Institute of Chemical Sciences, Heriot-Watt University, Edinburgh EH14 4AS, U.K.

[§]Eduard-Zintl-Institut für Anorganische und Physikalische Chemie, Technische Universität Darmstadt, Alarich-Weiss-Strasse 8, D-64287 Darmstadt, Germany

[∥]Australian Centre for Neutron Scattering, Australian Nuclear Science and Technology Organization, Locked Bag 2001 Kirrawee D.C., New South Wales 2232, Australia

S *Supporting Information*

ABSTRACT: The controlled catalytic functionalization of alkanes via the activation of C−H bonds is a significant challenge. Although C−H activation by transition metal catalysts is often suggested to operate via intermediate σ-alkane complexes, such transient species are difficult to observe due to their instability in solution. This instability may be controlled by use of solid/gas synthetic techniques that enable the isolation of single-crystals of well-defined σ-alkane complexes. Here we show that, using this unique platform, selective alkane C−H activation occurs, as probed by H/D exchange using D$_2$, and that five different isotopomers/isotopologues of the σ-alkane complex result, as characterized by single-crystal neutron diffraction studies for three examples. Low-energy fluxional processes associated with the σ-alkane ligand are identified using variable-temperature X-ray diffraction, solid-state NMR spectroscopy, and periodic DFT calculations. These observations connect σ-alkane complexes with their C−H activated products, and demonstrate that alkane-ligand mobility, and selective C−H activation, are possible when these processes occur in the constrained environment of the solid-state.

H/D exchange at a sigma–alkane complex
- Solid/gas single–crystal to single crystal–reactivity
- Selective C−H activation
- Single-crystal neutron diffraction on 3 isotopomers/isotopolgues
- Fluxional processes in the solid–state probed by periodic DFT & SSNMR
- **Directly connects σ−alkane complexes with C−H activated products**

INTRODUCTION

The controlled functionalization of alkanes via the activation of C−H bonds is of significant importance to the development of new methodologies that enable complexity to be introduced into simple fossil or bioderived natural resources or already-sophisticated molecules.[1−7] Catalytic methodologies using transition metal fragments offer the potential to dictate selectivity and reduce energetic barriers to such processes, for example, the selective dehydrogenation of alkanes to give olefins,[8−10] the upgrading of low-value light alkanes to higher-molecular weights for use as transportation fuels,[11−14] or the functionalization of alkanes to give valuable synthetic equivalents for further derivatization.[15,16] Aside from C−H functionalizations that operate via outer sphere or radical pathways, such as carbene[17] or oxo transfer reactions,[18] these processes are proposed to proceed via direct coordination of the alkane C−H bond with the metal center, engaging in a 3-center 2-electron interaction, i.e. a σ-alkane complex.[4,19−21] From such σ-complexes flow mechanistically distinct C−H activation pathways: σ-bond metathesis, C−H oxidative cleavage, and electrophilic activation (Scheme 1). Despite the accepted role of σ-alkane complexes as intermediates in these processes,[1,4,22−24] σ-alkane complexes are difficult to observe,

Scheme 1. C−H Activation via σ-Alkane Complexes[a]
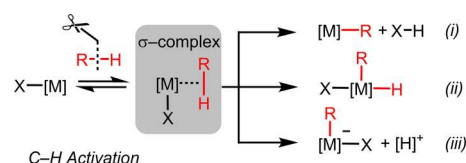
[a]Differentiation of common C−H activation processes: (i) σ-bond metathesis or related processes; (ii) oxidative addition (oxidative cleavage from the σ-alkane); (iii) electrophilic activation.

as, due to a combination of strong nonpolar C−H bonds and steric interactions from alkyl groups, alkanes are poor ligands, coordinating only weakly to metal centers.[1,25] Their direct observation generally relies upon generation in solution and detection *in situ* using low-temperature NMR spectroscopy and time-resolved infrared spectroscopy (TR-IR); either by photo-generation of the alkane complex by loss of, for example, a CO ligand or direct protonation of an Rh−alkyl bond.[26−30] Such observations build upon earlier matrix isolation experiments.[19]

Initially serendipitous single-crystal X-ray diffraction studies have shown alkane C−H bonds in close approach with metal centers (Fe^{2+},[31] U^{3+},[32] K^{+}[33]), in which host−guest interactions with alkane ligands are suggested to play an important role. Examples where a σ-alkane complex is observed which then undergoes C−H activation are even less common. Such species have been implicated from isotope labeling experiments,[22] dynamic processes in which an alkyl hydride is in rapid equilibrium with a σ-alkane complex,[34−36] or by direct observation using TR-IR that shows they are formed and then consumed by C−H oxidative cleavage over very short, e.g. nanosecond, time scales[24,37−39] (Scheme 2). The ability to

Scheme 2. Evidence for σ-Alkane Complexes in C−H Activation[a]

(a)

NMR Spectroscopy not observed E = H or D

(b)

Time−Resolved Infra-Red
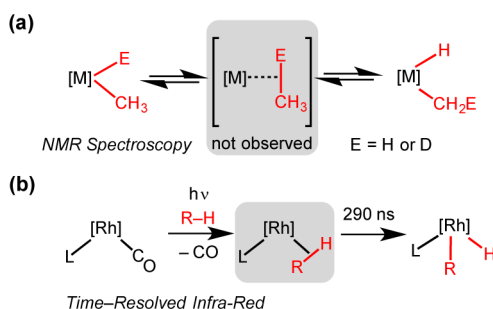
[a](a) Kinetically implicated σ-complexes in C−H activation, E = H, D;[42] (b) time resolved infrared techniques used to observe transient σ-complexes in C−H activation.[38] [Rh] = {Rh(*tris*-3,5-Me$_2$-pyrazolyl borohydride)}, L = additional ligand(s).

study the onward reactivity of well-defined σ-alkane complexes is thus limited, especially under standard laboratory conditions, but it would allow for their central role in C−H activation to be probed in detail. More common are H−H, B−H, Si−H, or intramolecular agostic C−H[20,40,41] activations that occur from relatively stable σ-complexes.

The instability of σ-alkane complexes can be attenuated by using single-crystal to single-crystal solid/gas[43−46] synthetic protocols; and we have recently established the utility of this approach for the synthesis of σ-alkane complexes of rhodium that can be characterized in the solid-state at, or close to, room temperature, for example [Rh(Cy$_2$PCH$_2$CH$_2$PCy$_2$)(η^2,η^2-C$_7$H$_{12}$)][BAr$^F_4$] (C$_7$H$_{12}$ = NBA, norbornane), **2** (Scheme 3).[47−49] We now show that by using this unique platform for

Scheme 3. Stable σ-Alkane Norbornane Complex, [Rh(Cy$_2$PCH$_2$CH$_2$PCy$_2$)(η^2,η^2-C$_7$H$_{12}$)][BAr$^F_4$], 2, Formed from a Solid/Gas Single-Crystal to Single-Crystal Reaction between H$_2$ and Norbornadiene Precursor, 1[48]

Single Crystal X−ray Diffraction *endo,exo*−H$_8$−**2** Stable (months)
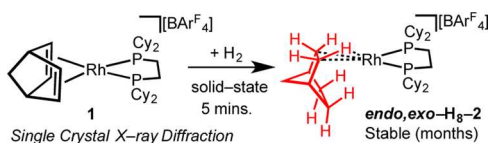
the study of σ-alkane complexes, selective and reversible C−H activation at the rhodium-bound NBA alkane ligand occurs, as probed by H/D exchange using exogenous D$_2$ in a solid/gas reaction, thus directly connecting a very well-defined σ-alkane complex to its C−H activation products. This selectivity can be harnessed so that five different isotopomers/isotopologues of
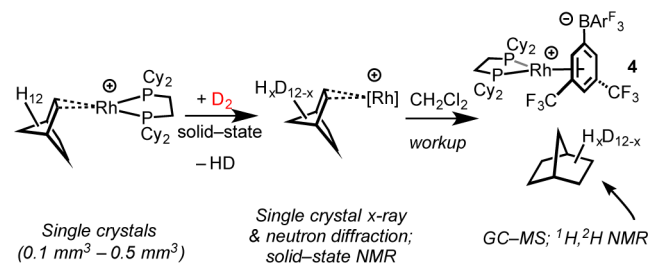
the σ-alkane complex can be formed. These selectivity patterns indicate a significant and unexpected mobility associated with the NBA−alkane ligand in the solid-state crystalline environment. This has been probed by variable-temperature single-crystal X-ray diffraction and solid-state NMR spectroscopy experiments, in concert with periodic DFT calculations that map out pathways for fluxional processes in the solid-state.

■ RESULTS AND DISCUSSION

C−H Activation Probed by H/D Exchange. We have previously reported that addition of H$_2$(g) to a crystalline sample of the bicyclic diene precursor [Rh(Cy$_2$PCH$_2$CH$_2$-PCy$_2$)(η^2,η^2-C$_7$H$_8$)][BAr$^F_4$], **1** [C$_7$H$_8$ = norbornadiene, NBD; Ar^F = 3,5-(CF$_3$)$_2$C$_6$H$_3$], results in the formation of the corresponding σ-alkane norbornane (NBA) complex [Rh-(Cy$_2$PCH$_2$CH$_2$PCy$_2$)(η^2,η^2-C$_7$H$_{12}$)][BAr$^F_4$], **2**, in the solid-state (Scheme 3)[48] by a single-crystal to single-crystal solid/gas reaction,[43,45] similar to the synthesis of the analogous complex [Rh(^{i}Bu$_2$PCH$_2$CH$_2$P^{i}Bu$_2$)(η^2,η^2-C$_7$H$_{12}$)][BAr$^F_4$], **3**.[47] Complex **2** is stable for months at 298 K under an inert atmosphere, whereas **3** is only stable below 253 K, transforming at 298 K to give a [BAr$^F_4$]-coordinated zwitterion and free NBA as the final products. In both **2** and **3**, an octahedral arrangement of [BAr$^F_4$]$^-$ anions provides a cavity that allows for these transformations within a crystalline "molecular flask,"[50] or nanoreactor.[51] Neither complex is stable on dissolution, even in very weakly coordinating solvents at very low temperatures (e.g., CDCl$_2$F/163 K[26,52]), liberating free NBA and forming the corresponding [BAr$^F_4$]$^-$ zwitterion, e.g. [Rh(Cy$_2$PCH$_2$CH$_2$-PCy$_2$){(η^6-C$_6$H$_3$-3,5-(CF$_3$)$_2$)BAr$^F_3$}], **4**.

This stability in the solid-state of **2** (Ar atmosphere, 298 K) coupled with the liberation of free NBA on dissolution allows for the reaction chemistry with regard to C−H activation at the coordinated alkane, as probed by H/D exchange with exogenous D$_2$, to be reliably studied (Scheme 4). Solid-state

Scheme 4. General Protocol for C−H Activation and Analysis of Products

Single crystals (0.1 mm^3 − 0.5 mm^3) *Single crystal x-ray & neutron diffraction; solid−state NMR* *GC−MS; ^{1}H,^{2}H NMR*

techniques, i.e. single-crystal neutron diffraction and solid-state NMR spectroscopy, do this directly, while solution techniques allow for the incorporated D atoms in the liberated NBA to be used as reporters in NMR spectroscopy and mass spectrometry.

Placing a single-crystalline sample of *endo,exo*-H$_8$-**2** (defined to emphasize the location of the key hydrogen positions of the NBA fragment) under an atmosphere of D$_2$(g) (2 atm, 298 K, ~10 equiv, 16 h) resulted in no change in single crystallinity, as measured by single-crystal X-ray diffraction. However, dissolution of this material in CH$_2$Cl$_2$ and analysis by ^{2}H NMR spectroscopy, or vacuum transfer of the NBA prior to analysis by ^{1}H NMR spectroscopy (CD$_2$Cl$_2$) and gas chromatography−mass spectrometry (GC-MS), revealed that a selective C−H activation process, that is H/D exchange, at the σ-bound NBA

Scheme 5. Synthesis and Characterization of the C−H Activated Products[a]

(a)

(b)   *exo*-D$_4$–NBA   *endo*-D$_4$–NBA   *endo,exo*-D$_8$–NBA

(c)
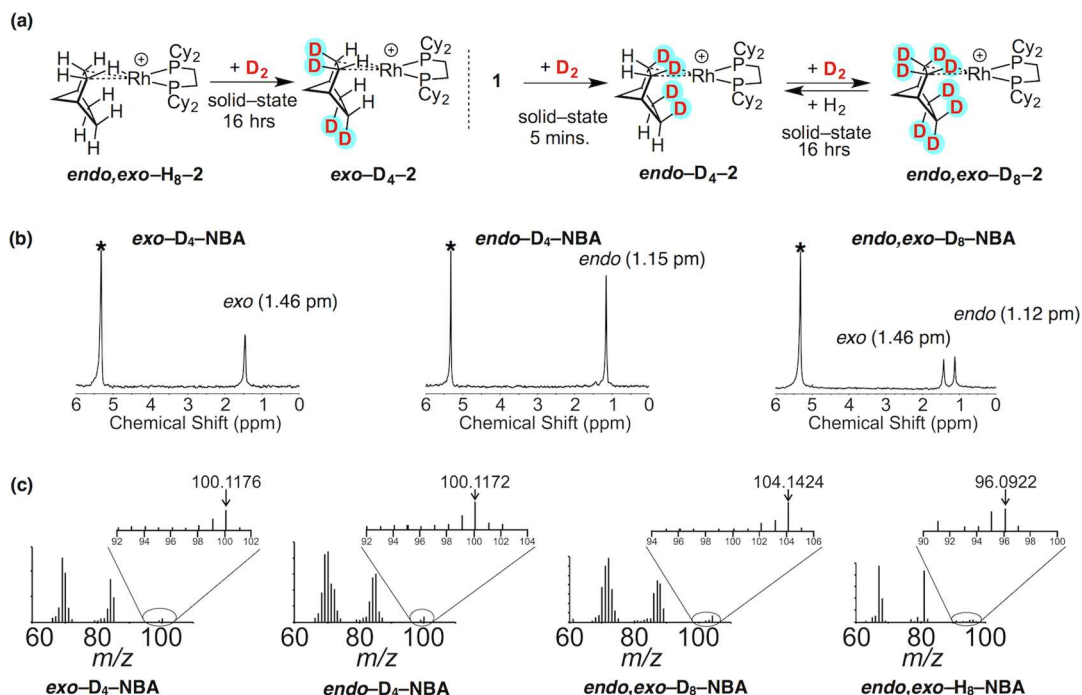
[a](a) Synthesis of the isotopologues/isotopomers starting from **1** and *endo,exo*-H$_8$-**2**, 298 K, [BAr$^F_4$]$^−$ anions are not shown; (b) ^{2}H NMR spectra (CH$_2$Cl$_2$) of the isolated NBA fragments [* = CD$_2$Cl$_2$ added as reference]; (c) GC-MS spectra with parent ions highlighted [H$_8$-NBA, C$_7$H$_{12}$ m/z = 96.0939 calcd].

Scheme 6. Single-Crystal Neutron Diffraction Derived Structures of the Products of C−H Activation[a]

Key: Cyan = positive nuclear density; magenta = negative nuclear density; white = H, red = D; orange = P; grey = C, teal = Rh
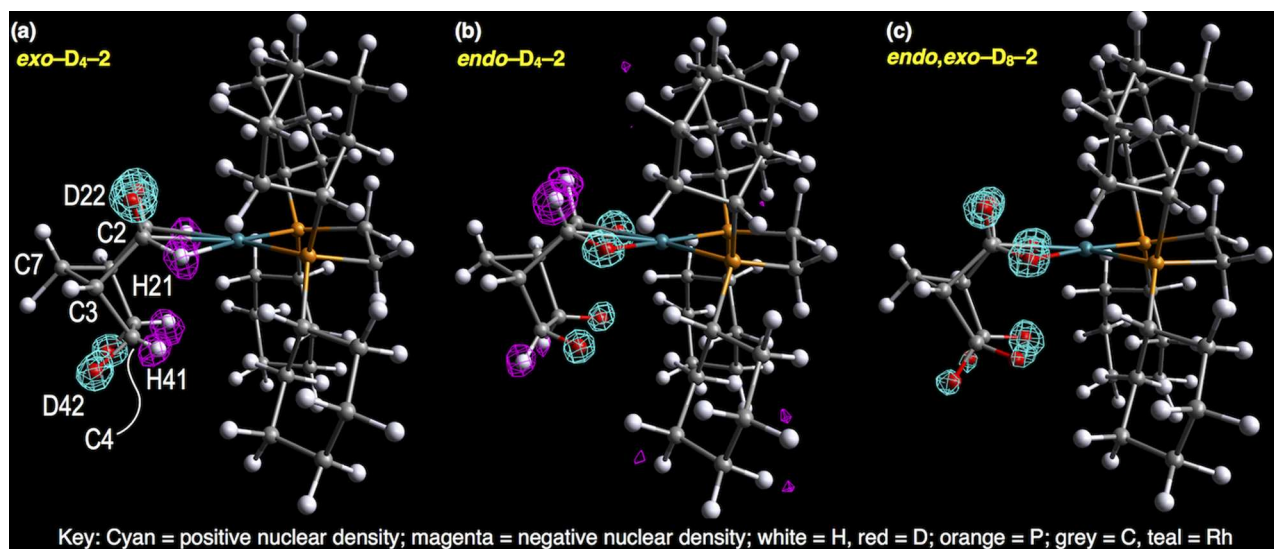
[a](a) *exo*-D$_4$-**2**; (b) *endo*-D$_4$-**2**; (c) *endo,exo*-D$_8$-**2**. Nuclear difference density contours are shown where the occupancy of H and D *exo* and *endo* atoms on the NBA fragment is set to zero. Coherent scattering factors: H = −3.7423(12) fm; D = +6.6749(6) fm. Temp = 150 K. Atoms shown at an arbitrary radius. See Supporting Information for details of contour levels.

fragment had taken place, as signaled by the liberation of *exo*-D$_4$-labeled NBA (Scheme 5).

The ^{1}H and ^{2}H NMR spectra of NBA and the *endo*-D$_2$-*exo*-D$_2$-NBA isotopologue have been previously reported.[53,54] In CD$_2$Cl$_2$ solvent the *exo*-protons of NBA are observed in the ^{1}H NMR spectrum at δ 1.47 and the *endo*-protons at δ 1.16 (Figure S8). In the ^{2}H NMR spectrum of the sample of dissolved *endo,exo*-H$_8$-**2** exposed to D$_2$(g) in the solid-state a single D-environment is observed at δ 1.46 with no signal at δ

~ 1.16 (detection limit ∼5% (Scheme 5b)). In the ^{1}H NMR spectrum, the corresponding resonance at δ 1.47 assigned to the *exo*-protons disappears. A GC-MS spectrum of the liberated NBA shows the parent ion at m/z = 100.1176 (calcd = 100.1190) with a fragmentation pattern very similar to NBA, albeit modified by ^{2}H incorporation, and a molecular weight consistent with the substitution of four hydrogen atoms with deuterium. Combined, these data suggest selective C−H activation in *endo,exo*-H$_8$-**2**, via H/D exchange, at the *exo*-

positions of the σ-bound alkane fragment to form *exo*-**D₄**-**2**. This selectivity is further underlined by the observation that exposure of *exo*-**D₄**-**2** to excess D_2 for 8 days results in no H/D exchange at the *endo*-positions to the detection limit of ^{2}H NMR spectroscopy of the dissolved sample.

Unambiguous determination of hydrogen and deuterium positions in the intact σ-alkane complex comes from single-crystal neutron diffraction of *exo*-**D₄**-**2** and, in particular, the very different scattering lengths, −3.7423(12) vs +6.6749(6) fm, of H and D, respectively (Scheme 6a). Single crystals (0.5 × 0.5 × 0.5 mm) were analyzed using Laue neutron diffraction at 150 K. A starting model based upon previously reported *endo,exo*-**H₈**-**2** derived from X-ray diffraction was used for the structural refinement.[48] There was essentially no change in unit cell or space group on addition of D_2 to *endo,exo*-**H₈**-**2** [P2₁/n, V = 6691.62(9), cf. 6695.46(7) Å³] as determined by single-crystal X-ray diffraction. For the neutron-diffraction refinement, although restraints were applied to the remote phosphine substituents, the NBA fragment was freely and isotropically refined including all the hydrogen sites associated with the alkane fragment. Initial refinement using all ^{1}H scattering factors yielded a poor fit to the data and an unstable refinement [R = 24.0%], which was improved substantially by replacement of all four *exo*-hydrogens with deuterium [R = 15.2%]. Replacement of all the *endo*- and *exo*-hydrogens, or just the *endo*-hydrogens, with deuterium, resulted in a poor fit to the data and an unstable refinement [R = 26.6% and 30.2%, respectively]. Setting occupancies of *endo*- and *exo*-positions to zero and inspection of the difference Fourier map showed significant regions of positive density, i.e. deuterium, in the four *exo*-positions and significant regions of negative density in the four *endo*-positions, i.e. hydrogen, as shown in Scheme 6a. Due to the large unit cell, which is approaching the practical application limit of the KOALA Laue neutron diffractometer (see Supporting Information),[55] and the relatively low data:parameter ratio, which is diminished by the required modeling of the large disordered [BArF₄]⁻ anion, we note only that the key structural metrics for the C—H bonds follow the typical trend[56] of being rather longer than those reported from X-ray data [e.g., C2—H21 = 1.18(5), C2—D22 = 1.03(3) Å, neutron; cf. 0.99(4), 0.97(4) Å, X-ray]. The data clearly yield an unambiguous determination of the locations occupied by hydrogen and deuterium, confirming the selectivity for C—H activation. Crucially, this selectivity is confirmed and quantified by the complementary techniques of solution NMR spectroscopy and GC-MS, that demonstrate that the isotopologue *exo*-**D₄**-**2** is formed selectivity upon H/D exchange with *endo,exo*-**H₈**-**2**. Thus, *all four exo*-C-H positions in the starting NBA complex have undergone H/D exchange, leaving the *endo*-C-H hydrogens that are coordinated through 3-center 2-electron σ-interactions with the rhodium center unmodified. The selective activation of these remote C—H positions was unexpected. Intramolecular C—H activation in organometallic complexes in the solid−state has been reported before, but not in single-crystal to single-crystal transformations.[43,57−61] We have previously reported H/D exchange in the solid-state at coordinated NH₃ by addition of D_2 to [Rh(^{i}Bu₂PCH₂CH₂-P^{i}Bu₂)(NH₃)₂][BArF₄].[62]

Although neutron diffraction studies on σ-complexes have been reported, such as those involving dihydrogen, silanes, or boranes,[63−66] those on (partially) deuterated samples are particularly rare. For example, single-crystal structure determinations of the products of solution-phase intramolecular C—H

activation via H/D exchange in Ru{P(C₅H₉)₃}₂(H)₂(η²-H₂)₂ reveal selective C—H activation at the phosphine alkyl groups to give Ru{P(C₅H₇D₂)₃}₂(D)₂(η²-D₂)₂.[67] H/D exchange in the alkyl phosphine occurs at the position that would be expected to directly engage in an (unobserved) agostic Ru···H−C interaction prior to C—H cleavage, i.e. the C—H groups that are directed toward the metal center. The only neutron diffraction study on σ-alkane interactions comes from very low-temperature (less than 10 K) *powder* diffraction studies on metal−organic frameworks with unsaturated metal sites (e.g., Fe,[68] Co,[69] Cu[70]) that are doped with CD₄, C₂D₆, or C₃D₈. No single-crystal neutron studies on σ-alkane complexes have been reported.

Addition of D_2 (2 atm, 298 K) to single-crystals of **1** resulted in the rapid (10 min) deuteration of the diene and formation of *endo*-**D₄**-**2**. D_2 addition across the double bonds occurs with ~95% selectivity[71] to give the isotopomer of *exo*-**D₄**-**2**, as shown by GC-MS and ^{1}H and ^{2}H NMR spectroscopy of the liberated NBA (Scheme 5), as well as a single-crystal neutron diffraction study (Scheme 6b). This selectivity is in contrast to D_2 addition to related NBD complexes in solution,[53,54] including **1**, or the solid/gas synthesis of **3**[47] (the ^{i}Bu analog of **2**), that liberate the *endo*-**D₂**-*exo*-**D₂**-NBA isomer (Scheme 7). In these examples, the first addition of D_2 proceeds with

Scheme 7. Isotopomers of *d₄*-NBA Formed Depending on the System
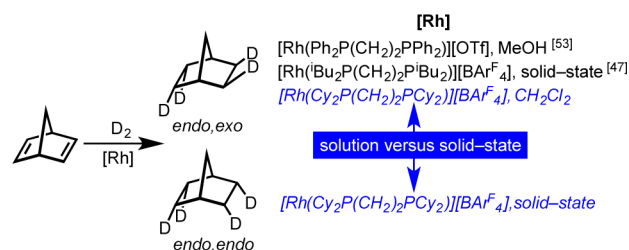
endo-selectivity, and the resulting norbornene intermediate—that also likely contains an agostic C—H interaction[47,72]—rearranges to present the *exo*-alkene face to the metal, from which follows *exo*-addition of D_2 to the remaining C=C double bond. For the cyclohexyl-substituted **1**, such mobility in the solid-state to form the analogous intermediate NBE complex must be relatively high energy compared with D_2 addition, and *endo*-selectivity results (*vide infra*). This demonstrates that the confined environment defined by the [Rh(L₂)]⁺/[BArF₄]⁻ pairing in the solid-state can result in significant changes in the chemoselectivity of D_2 (and thus likely H_2) addition, as shown by the reluctance for the NBE-intermediate to rearrange to present an *exo*-alkene face in D_2 addition to **1**. No H/D exchange occurs in solution when D_2 (2 atm, 16 h) is added to a 1,2-F₂C₆H₄ solution of [Rh-(Cy₂PCH₂CH₂PCy₂)(η⁶-F₂C₆H₄)][BArF₄][49]/NBA, as expected given that we have shown that NBA does not bind with the metal fragment in solution, even at very low temperatures.[48]

An independent synthesis of this putative *exo*-NBE complex **5** (see Supporting Information for details and single-crystal X-ray structure) reveals the expected[47,72] NBE coordination mode, via the alkene and Rh···H−C(7) interactions. Addition of D_2 in the solid-state (2 atm, 5 min) gives *exo*-**D₂**-**2**, as measured by GC-MS and NMR spectroscopy of the liberated NBA (Scheme 8), showing that, if formed, **5** would give the expected *exo*-selectivity for D_2 addition. Leaving a sample of **5**

**Scheme 8. Addition of D$_2$ to a Norbornene Precursor, 5**
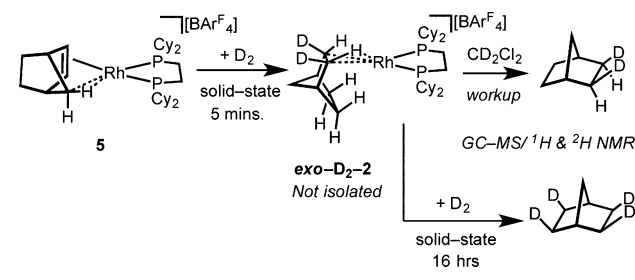
under D$_2$ overnight and subsequent workup liberates NBA as the *exo*-D$_4$-2 isomer, that arises from *exo*-H/D exchange in *exo*-D$_2$-2. That ~95% selectivity is observed for the addition of D$_2$ to 1 argues against 5 being a significant intermediate en route to 2. Addition of H$_2$ to single crystals of 5 resulted in a single-crystals to single-crystal transformation to give *endo,exo*-H$_8$-2, which was analyzed using single-crystal X-ray diffraction. Although the quality of the data was poorer than when synthesized from 1, the connectivity of the resulting σ-alkane complex was confirmed. Interestingly, the structure of 5 as determined by single-crystal X-ray diffraction shows that the NBE ligand is disordered in the solid-state between two chemically equivalent, but crystallographically distinct, orientations of the NBE ligand in which the alkene and agostic Rh···H−C interactions are swapped. The disorder is modeled by a 1:3 relative population. As the ^{31}P{^{1}H} SSNMR spectrum (298 K) of 5 shows signals assigned to both these components, this suggests that if there is a fluxional process occurring it must be slow relative to the NMR timescale at 298 K, and thus has an appreciable barrier.

The availability of *endo*-D$_4$-2 allows for the synthesis of the isotopologue *endo,exo*-D$_8$-2 (Scheme 5) by further addition of D$_2$ overnight. The ^{2}H NMR spectrum of the resulting, liberated, NBA reveals two signals of equal integration (δ 1.43, 1.12), that correspond to the *exo* and *endo* C−D positions, respectively. GC-MS shows a parent ion at *m/z* = 104.1424 (calcd 104.1414), demonstrating eight deuteriums in total have been installed onto the NBA ligand by the sequential solid/gas^{43,44,73,74} processes: 1 to *endo*-D$_4$-2 to *endo,exo*-D$_8$-2. A single-crystal neutron diffraction study on single-crystals obtained in this manner confirmed the substitution pattern, showing deuterium at all eight *endo/exo* positions of the NBA (Scheme 6c). As expected, addition of H$_2$ to *endo,exo*-D$_8$-2 in a solid/gas single-crystal to single-crystal reaction resulted in the formation of *endo*-D$_4$-2, as characterized by GC-MS/NMR spectroscopy of the liberated NBA fragment and ^{2}H SSNMR (Scheme 5).

These results demonstrate that in every case C−H (or C−D) activation occurs selectively at the remote *exo*-C−H (C−D) position of the bound methylene unit of the NBA even though it is the *endo*-C-H groups that partake in the σ-interaction with rhodium. To the detection limit of NMR spectroscopy, C−H activation at the bridge (C7) or bridgehead (C3/C6) positions, the phosphine ligand, or the [BAr$^F_4$]$^-$ anion does not occur, as measured in solution of the resulting free NBA and the zwitterion 4. Furthermore, all four *exo*-positions on the NBA undergo C−H activation, even though the ground-state structure determined by single-crystal diffraction shows that only one pair (i.e., that associated with C1 and C2, Scheme 6a) are bound with the metal center. This suggests fluxional

processes are occurring in the solid-state at 298 K^{75} that make all the *exo* positions accessible for C−H activation.

Fluxional Processes in the Solid−State. Assuming a Rh(I) manifold, four possible fluxional processes for the NBA ligand are outlined in Scheme 9: *pivot, C$_2$-rotation, rock,* and

Scheme 9. Possible Fluxional Processes Occurring in the Solid-State for the NBA Fragment^a
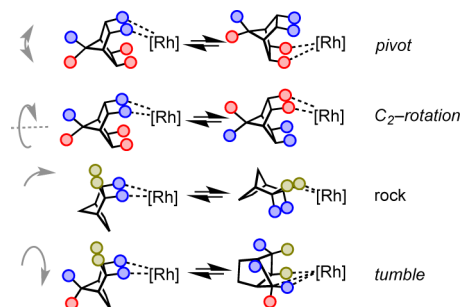
^{a}Selected hydrogen atoms are shown as filled circles, colored to guide the eye. [Rh] = {Rh(Cy$_2$PCH$_2$CH$_2$PCy$_2$)$^+$.

tumble. The *C$_2$-rotation* is degenerate and, thus, invisible to diffraction techniques, as has been noted previously for fluxional processes occurring in the solid-state for metallocene-type complexes.^{76} In contrast, *pivot, rock,* and *tumble* would imply the observation of disorder in the single-crystal structures, if these processes led to an appreciable population of an alternative isomer.^{77,78} That such isomers do not contribute significantly to the ground state structure even at higher temperatures is demonstrated by a single-crystal X-ray structure of *endo,exo*-H$_8$-2 determined at 290 K (Figure 1a) that showed no disorder within the cation; the C−C and Rh···C distances remained unchanged within error compared to the previously reported structure determined at 150 K.^{48}
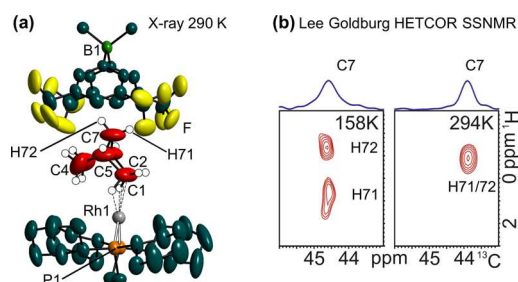

Figure 1. (a) Single-crystal X-ray diffraction structure at 290 K of *endo,exo*-H$_8$-2, with selected H atoms shown, showing the relationship with the [BAr$^F_4$]$^-$ anions (selected aryl rings shown). Selected bond distances (Å) [150 K distances^{48}]: Rh1−C1, 2.402(5) [2.389(3)]; Rh1−C2, 2.412(6) [2.400(3)]; C1−C2, 1.544(9) [1.552(4)]; C4−C5, 1.548(13) [1.546(7)]. Only the largest disordered component of each of the CF$_3$ groups is shown. (b) 158 and 294 K ^{1}H/^{13}C frequency-switched Lee−Goldburg HETCOR SSNMR (10 kHz) of *endo,exo*-H$_8$-2 highlighting the NBA bridge-CH$_2$ group, C7.

These fluxional processes have also been probed by variable-temperature solid-state NMR experiments (SSNMR). For three of these processes—*pivot, rock,* or *tumble*—the CH$_2$ protons associated with the bridge methylene (C7) would remain inequivalent, whereas a *C$_2$-rotation* would make them equivalent if faster than the NMR time scale. A frequency-switched Lee−Goldburg (FSLG) ^{1}H−^{13}C HETCOR SSNMR

experiment on ***endo,exo*-H$_8$-2** allows for the ^{1}H NMR projection to be indirectly detected, for which we have previously shown reasonable agreement between calculated and experimental chemical shifts.[48] At 294 K this reveals a single proton environment, centered at δ −0.8, identified as the methylene group of the NBA bridge C7 [$\delta(^{13}$C)44], which sits in the cleft of two BAr$^F_4$ aryl rings (Figure 1) and thus experiences a ring current, as we have previously noted.[48] It is now apparent that this single ^{1}H environment observed at 294 K is due to a C_2-*rotation* exchange process in the solid-state that is fast on the NMR time scale at this temperature and makes the crystallographically distinct H71 and H72 equivalent [one sits pointing into the aryl-cleft (H72) while one is orientated to one side]. Progressive cooling of the sample to 158 K results in this signal splitting into two environments in the ^{1}H-projection [H72, H71; δ −1.4, 0.4] (Figure 1b), fully consistent with the solid-state structure. These chemical shifts now offer an excellent agreement with those calculated applying the GIPAW method on the extended solid-state structure [δ −1.2, 0.3]. At the intermediate temperature of 200 K these correlations are lost and the ^{13}C{^{1}H} SSNMR spectrum is broad. These changes are reversible on warming, consistent with the halting of a C_2-*rotation* fluxional process of the bound NBA ligand at 158 K. Assuming that the coalescence temperature for the two peaks occurs at approximately 200 K, from the peak separation at 158 K ($\Delta\nu$ = 772 Hz), the rate constant is $k_r \leq 1.7 \times 10^3$ and the activation energy barrier ($\Delta G^{\ddagger}$) at 200 K is ca. 9 kcal/mol.

Although the protons associated with C7 are resolved well at 158 K in the FSLG ^{1}H–^{13}C HETCOR SSNMR experiment, the high-field Rh···H−C hydrogens are not (Supporting Information). In order to probe this fluxional process further and also determine the chemical shifts associated with the $\sigma-$ Rh···H−C interaction, the corresponding ^{2}H MAS-SSNMR experiments at 110 K of ***endo*-D$_4$-2**, synthesized by addition of H$_2$ to ***endo,exo*-D$_8$-2**, were run that did allow for their observation (Figure 2). At this temperature any fluxional processes are halted. The resulting difference spectrum, in which a small contribution of mobile ***endo*-D$_4$**-NBA that arises from decomposition during sample transport/preparation is subtracted, consists of two subspectra. These can be deconvoluted to give two sets of NMR parameters: δ_{iso} 0.7 [Q_{cc} = 171 kHz, $\eta_q \approx 0$] and δ_{iso} = −3.5 [Q_{cc} = 123 kHz, η_q = 0.4]. The former values are typical for immobile C−D groups. The latter parameter set signals M···D−C interactions, where quadrupolar coupling (Q_{cc}) and asymmetry (η_q) parameters lie in-between the values expected for a C−D group (ca. 170 kHz, 0) and those measured and calculated for bridging deuterides (ca. 80−100 kHz, ∼0.8).[79,80] Importantly, these observed parameters also fit very well with those calculated using the GIPAW method (Figure 2c). Increasing the temperature to 298 K results in a change of line shape consistent with the onset of mobility. This is strongly supported by a spectrum measured at 218 K, where almost no signal is observable, most probably due to very short T$_2$ relaxation in this temperature region.[81,82] By comparison with ***endo*-D$_4$-2**, for ***exo*-D$_4$-2** only one component is observed at 110 K [δ_{iso} = 1.1], with a large Q_{cc} = 171 kHz and a small η_q = 0.02, as might be expected for chemically similar C−D bonds that do not interact with a metal center (Supporting Information). Presumably this single environment is a coincidence of the four discrete environments, as confirmed by calculated parameters being very similar for all four deuterons: $\delta_{iso} \sim$ 1.7 [Q_{cc} = 182 kHz, $\eta_q \approx$ 0.01].
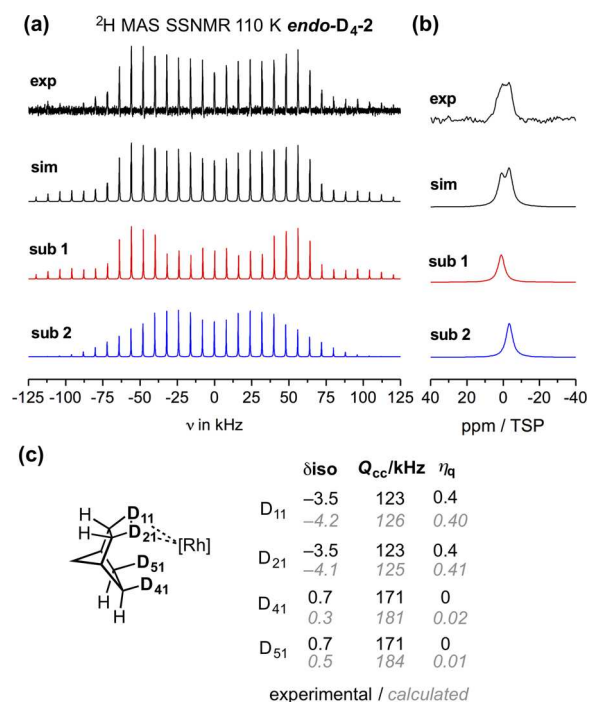

Figure 2. Experimental and simulated ^{2}H MAS difference spectrum at 8 kHz spinning at 110 K of ***endo*-D$_4$-2**. (a) Experimental spectrum (exp), simulated spectrum (sim), sub spectrum 1 (sub 1), and sub spectrum 2 (sub 2). (b) Details of the isotropic signal referenced to trimethylsilyl propionate (TSP). (c) Comparison of experimental and calculated (italics, CASTEP/GIPAW) parameters for ***endo*-D$_4$-2**.

All four fluxional processes have been modeled in the solid-state using periodic DFT calculations at the PBE-D3 level. As found previously,[49] geometry optimization with this approach provides good agreement with experiment, and this is also the case for **2** (see Table S2, Supporting Information, and Figure S47 for an overlay of experimental and computed structures). Of the four possible pathways, the C_2-*rotation* (Scheme 10) proved most accessible with an overall barrier of 9.5 kcal/mol, in very good agreement with the barrier estimated from SSNMR spectroscopy (9 kcal/mol). This process involves an intermediate, **2$_{rot}$**, at +5.2 kcal/mol that features an η^2: η^2-NBA ligand bound through the H21−C2 and H41−C4 bonds with Rh···H21 and Rh···H41 distances of 1.91 and 1.92 Å, respectively (see Scheme 10c−f for the computed structures). Relative to **2**, the NBA ligand in **2$_{rot}$** has rotated by 74°, as quantified by ϕ, the angle between the {H71C7H72} and {P1RhP2} planes. **2$_{rot}$** is accessed via **TS$_{rot-1}$** (ϕ = 50.9°), in which some weakening of the initial Rh···H21 interaction is compensated by shortening of both the Rh···H41 and Rh···H51 distances. C_2-*rotation* is completed via **TS$_{rot-2}$** (ϕ = −27.4°), which features three Rh···H contacts below 2.25 Å. The different structures of **TS$_{rot-1}$** and **TS$_{rot-2}$** reflect the anisotropy of the cavity within which the C_2-*rotation* is proceeding, and their degeneracy is purely coincidental. These different structures also reflect the flexibility of the Rh-NBA interaction within the cavity. Following **TS$_{rot-2}$** regenerates **2**, thus completing the degenerate C_2-*rotation* process.

Details of the *pivot* and *rock* processes are given in Scheme 11. These involve a single step, with barriers of 11.1 and 13.9 kcal/mol, respectively, and the transition states both exhibit four Rh···H−C close contacts, either through the *endo*−C-H bonds (**TS$_{pivot}$**, Rh···H−C: 2.14 Å − 2.36 Å) or via a *bis-*

Scheme 10. Details of the C_2-rotation Computed in the Solid-State via Periodic DFT Calculations^a
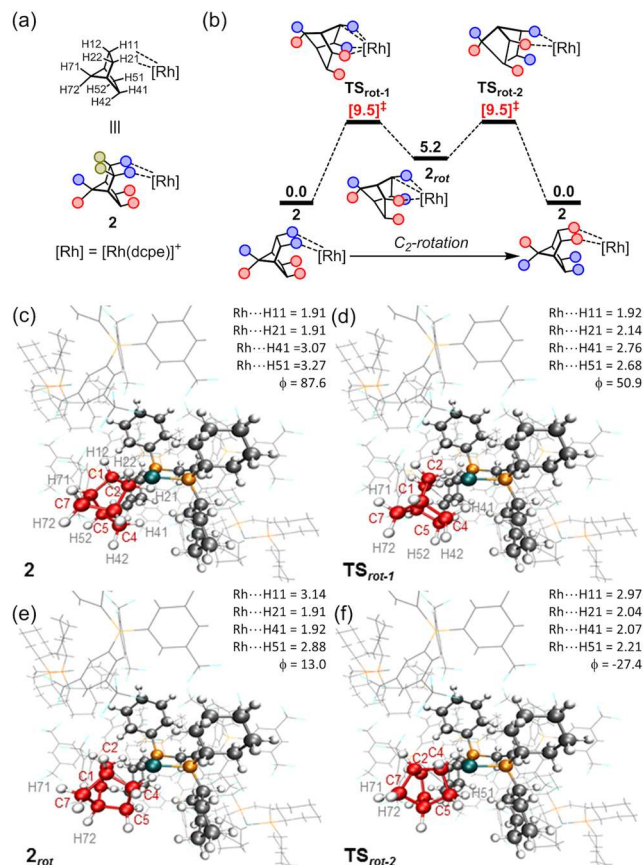
^{a}(a) H atom labeling scheme. (b) Energy profile. (c–f) Geometries of stationary points Rh···H, distances in Å and ϕ (the angle between the {H71C7H72} and {P1RhP2} planes) in degrees. All energies in kcal/mol; method: [CP2K] PBE-D3/DZVP-MOLOPT-SR-GTH/GTH-PBE (cutoff 500 Ry).

bifurcated structure (**TS$_{rock}$**, Rh···H–C: 2.18–2.44 Å). Pivoting leads to η^2:η^2 endo-bound **2$_{pivot}$** (Rh···H41 = 1.88 Å; Rh···H51 = 1.89 Å). Significantly, the molecular cation in **2$_{pivot}$** is structurally equivalent to that in **2**, but **2$_{pivot}$** is destabilized by 9.2 kcal/mol due to the now unfavorable position of the NBA ligand within the cavity. **TS$_{rock}$** leads to η^2:η^2 exo-bound **2$_{rock-1}$** at +9.7 kcal/mol with Rh···H12 = 1.82 Å and Rh···H22 = 1.85 Å.
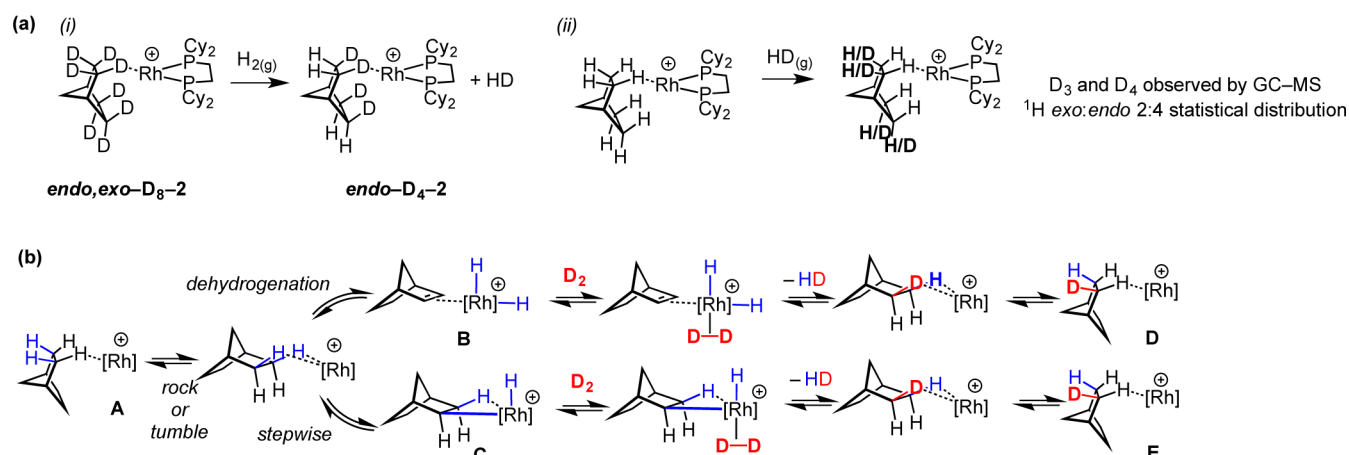
In contrast to the other processes, the NBA *tumble* starts from intermediate **2$_{rock-1}$**, and from here it can proceed with either a clockwise (viewed from Rh) or an anticlockwise motion of the NBA. The lower energy clockwise rotation (Scheme 11b) produces a new η^2:η^2 isomer, **2$_{tumble-1}$**, at +6.6 kcal/mol, in which the NBA is bound through the *exo*-H22-C and H71-C from the bridging methylene group (see also Scheme 11d). Movement of Rh from H22 to H21 via **TS$_{wag}$** produces **2$_{tumble-2}$** at +7.8 kcal/mol (Scheme 11e), from which a further clockwise tumble generates η^2:η^2 exo-bound **2$_{rock-2}$** (+3.5 kcal/mol).

Schemes 10 and 11 show that several isomers of **2** can be accessed via nondegenerate rearrangement of the NBA ligand within the cavity. However, none of these are sufficiently stable to be observed, for instance via the manifestation of disorder in

Scheme 11. Details of the *pivot*, *rock*, and *tumble* Computed in the Solid-State via Periodic DFT Calculations^a
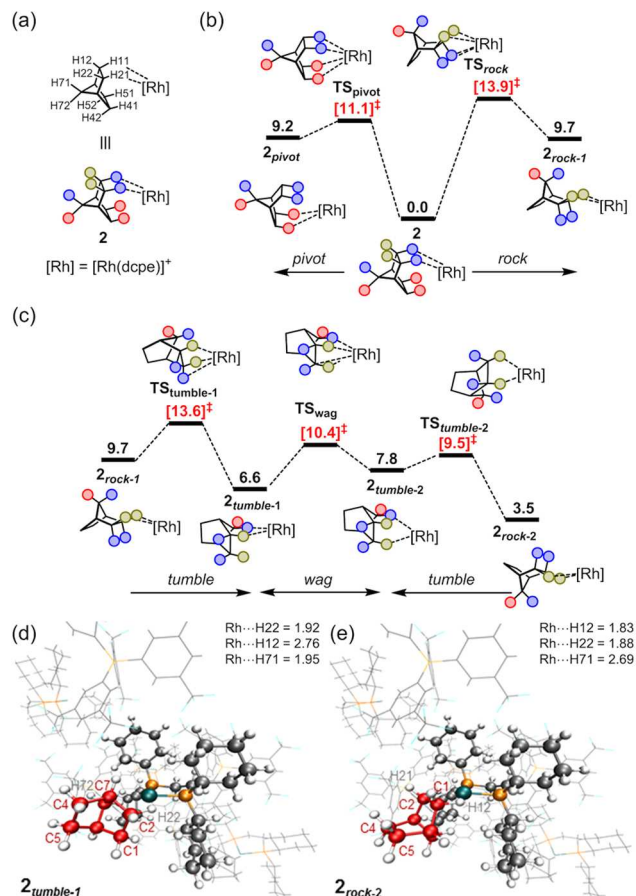
^{a}(a) H atom labeling scheme. (b) *Pivot* and *rock* energy profiles. (c) *Tumble* energy profile starting from intermediate **2$_{rock-1}$**. (d and e) Geometries of selected stationary points with Rh···H distances in Å. All energies in kcal/mol. Details of all other stationary points are provided in the Supporting Information. Method: [CP2K] PBE-D3/DZVP-MOLOPT-SR-GTH/GTH-PBE (cutoff 500 Ry).

the crystal structure of **2**. The degenerate C_2-rotation is the most accessible fluxional process, and it is the slowing of this rearrangement that accounts for the nonequivalence of H71/H72 at low temperature. At room temperature the *exo*-bound isomers (**2$_{rock-1}$** and **2$_{rock-2}$** as well as **2$_{tumble-1}$** and **2$_{tumble-2}$**) will be kinetically accessible, and any one of these could provide a starting point for the *exo*-selective C–H activation process. The extended crystal environment is crucial in determining the energetics of these various species. This is underlined upon recomputing the equivalent minima as isolated cations, in which form they all lie within 5.2 kcal/mol of each other; indeed, with this model **2$_{pivot}$** actually lies slightly below **2** (see Supporting Information). Variations in the precise environment provided by the solid-state are also a key factor; for example, for **3** (the ^{i}Bu analogue of **2**) the alternative η^2:η^2 endo-bound form **3$_{pivot}$** lies only 1.7 kcal/mol above the ground state. In this case, the experimentally determined crystal structure does indeed show disorder, with NBA components equivalent to those in **3** and **3$_{pivot}$**.[26] These fluxional processes, characterized here in the solid-state, are directly analogous to chain-walking events,[28,42,52,83] and selective binding of axial C–H bonds

Scheme 12. Experimental Evidence, and Suggestions for, the Mechanisms of C–H Activation[a]

[a](a) (i) Addition of H_2 to ***endo,exo*-D$_8$-2** to form ***endo*-D$_4$-2** and HD; (ii) Addition of HD to ***endo,exo*-H$_8$-2**. (b) Suggested mechanisms for H/D exchange based on observed isotope distribution and isotope-labeling experiments.

over equatorial C–H bonds,[84] as observed using NMR spectroscopy at low-temperature in solution for transient σ-alkane complexes. Such processes generally have barriers estimated to be between 5 and 12 kcal/mol. We have recently remarked upon similar barriers for the proposed chain walking of a σ-bound pentane ligand in the solid-state.[49]

Comments on the Mechanism of C–H Activation. This selectivity for C–H activation at the *exo*-position is unexpected and remarkable, and experiment and computation provide insight into the likely palette of mechanistic pathways. That the *exo*-C–H positions are selectively activated even though the ground state-structure shows *endo*-C–H coordination points to Curtin–Hammett conditions for productive C–H activation. Furthermore, H/D scrambling between *exo* and *endo* sites does not occur, as no mixed *endo/exo* isotopomers are observed. This excludes intramolecular H/D exchange processes[23] and mechanisms involving double C–H activation at one carbon, i.e. via a carbene dihydride.[2] H/D exchange also occurs in the dark, excluding a photochemical mechanism. Rh-hydride (deuteride)-containing intermediates are indirectly signaled by the observation of HD [δ 4.57, 1:1:1 triplet, J(HD) = 42 Hz] in the NMR spectrum of dissolved headspace when single-crystals of ***endo,exo*-D$_8$-2** are exposed to H$_2$(g) to form ***endo*-D$_4$-2** (Scheme 12a). Such intermediates could arise from *exo* C–H oxidative cleavage of the bound NBA in the starting complex, e.g. ***endo,exo*-H$_8$-2** (A, Scheme 12b), to give a norbornyl-hydride intermediate C (stepwise C–H activation), or oxidative cleavage followed by β-hydrogen transfer to give dihydride B (dehydrogenation).[52] After exchange with D$_2$[20,85] these collapse back to give partially deuterated σ-alkane complexes E and D. Under an excess of D$_2$, and assuming similar barriers to C–H activation for all the *exo*-CH bonds rendered accessible by the C_2-rotation and *rock/tumble* fluxional processes, D and E would then proceed to give the final product, i.e., ***exo*-D$_4$-2**. Intermediate B could be formulated as a dihydrogen tautomer, but arguing against this is the observation of the D$_3$ and D$_4$ isotopologues by GC-MS when HD(g) is added to ***endo,exo*-H$_8$-2**. These would not be formed if bound H$_2$ was simply substituted by exogenous HD. Proposed intermediate C is closely related to group-10 norbornyl complexes [M-(Cy$_2$PCH$_2$CH$_2$PCy$_2$)(σ,η^2-C$_7$H$_{11}$)][BF$_4$] (M = Pd, Pt) that

show agostic M···H–C interactions,[86] while site-exchange of bound ethane in [Ir(PONOP)(η^2-H$_3$CCH$_3$)][BAr$^F_4$] [PONOP = 2,6-(^{t}Bu$_2$PO)$_2$C$_5$H$_3$N] has been proposed to occur via a reversible dehydrogenation pathway similar to intermediate B.[52] If intermediate B was being formed, there also must be a significant barrier to NBE rearrangement (i.e., to present the *endo* face) to account for the observed selectivity. Although studies on 5 point to this, the comparison with B should be viewed cautiously given the difference in oxidation states between the two and the presence of exogenous D$_2$ (or H$_2$) under conditions of H/D exchange. We also cannot rule out alternatives that involve initial D$_2$ oxidative addition to give a Rh(III) dideuteride σ-alkane intermediate followed by H/D exchange via a σ-complex assisted metathesis process.[20] Computational studies to provide a full exploration of these mechanistic possibilities in the solid-state are currently underway.

CONCLUSIONS

We have shown that by using the platform of solid/gas single-crystal to single-crystal transformations, alkane C–H activation at a well-defined σ-alkane complex can occur, as probed by H/D exchange using D$_2$. These observations not only connect σ-alkane complexes with their C–H activated products but also demonstrate that alkane-ligand mobility, and selective C–H activation, are possible when these processes occur in the constrained environment of the solid-state. Although the precise mechanism for C–H activation is yet to be determined, it is likely that the solid-state environment enables the high levels of selectivity observed for C–H activation. This encourages the further development of solid/gas organo-metallic techniques for the selective and catalytic functionalization of alkanes using well-defined organometallic complexes, and it will be interesting to explore whether a σ-alkane complex, such as 2, acts as precatalyst for such processes.

EXPERIMENTAL SECTION

Synthesis of *exo*-D$_4$-2. A crystalline sample of 1[48] (ca. 20 mg) was loaded into a J. Youngs flask in an argon-filled glovebox. Subsequently, the flask was placed under H$_2$ gas (2 atm) to form ***endo,exo*-H$_8$-2** (not isolated). The reaction was left for 15 min before the H$_2$ gas was removed by exposure to vacuum (less than 1 × 10^{-2} mbar) and

replaced with D_2 gas (2 atm). The crystals were left under this atmosphere overnight, forming *exo*-D_4-**2**. The D_2 was then removed by exposure to vacuum and replaced with an atmosphere of Ar.

Synthesis of *endo*-D_4-2. (A) A crystalline sample of **1** (ca. 20 mg) was loaded into a J. Young's flask in an argon-filled glovebox. This was placed under a D_2 atmosphere (2 atm). The reaction was left for 5 min before the D_2 gas was removed by exposure to vacuum (less than 1×10^{-2} mbar) and the crystals were left under an atmosphere of Ar. (B) A crystalline sample of *endo,exo*-D_8-**2** was loaded into a high pressure NMR tube in an argon glovebox. This was placed under an atmosphere of H_2 (2 atm, overnight) to form *endo*-D_4-**2** before the H_2 gas was removed by exposure to vacuum (less than 1×10^{-2} mbar) and the crystals were left under an atmosphere of Ar

Synthesis of *endo,exo*-D_8-2. A crystalline sample (ca. 20 mg) of **1** was loaded into a J. Young's flask in an argon-filled glovebox and subsequently put under 2 atm of D_2 gas overnight. The next day the atmosphere was removed by exposure to vacuum (less than 1×10^{-2} mbar) and the sample was placed under argon.

Laue Neutron Diffraction Data Collection and Reduction. The Laue single-crystal neutron diffraction studies reported were each undertaken using the KOALA instrument standing at the end guide position of TG3.[55] An unmonochromated thermal neutron beam produced from the OPAL reactor at the Australian Nuclear Science and Technology Organization was incident on a crystal mounted to the φ axis of the instrument, and the diffraction patterns were recorded on neutron sensitized "Niimura special" image plates mounted to the fixed radius cylindrical detector drum. All samples were handled immersed in argon to ensure compound stability while the crystal was transferred to the cold nitrogen stream of an Oxford Cryosystems COBRA cryostream. Details of the individual data collection and reduction procedures are provided in the relevant CIFs and Supporting Information. All crystals are monoclinic, and data from two separate orientations of the unit cell with respect to the phi axis of the instrument were recorded to ensure full coverage of the unique fraction of reciprocal space.

Solid-State ^{2}H MAS NMR Spectroscopy. All ^{2}H solid-state MAS experiments were performed on a Bruker AVANCE III 400 DNP spectrometer which is equipped with a low-temperature MAS unit and a three channel H/X/Y probe. ^{2}H was measured at 9.4 T, corresponding to a frequency of 61.41 MHz. Spectra were recorded at 8 kHz spinning at nominally 110 K. All spectra were referenced to TSP (trimethylsilyl propionate, 0 ppm) measured at RT. Single pulse experiments were performed employing a 90° excitation pulse of 3.5 μs and a repetition delay of d1 = 0.5 s to d1 = 100 s.

Periodic DFT Calculations. Periodic electronic structure geometry optimizations were carried out at the PBE-D3 level of theory, employing the Gaussian plane wave (GPW) formalism as implemented in the QUICKSTEP module within the CP2K program suite (Version 2.7). NMR parameters were modeled using the GIPAW method as implemented in CASTEP 8.0. See Supporting Information for full details and references.

■ ASSOCIATED CONTENT

Ⓢ Supporting Information

The Supporting Information is available free of charge on the ACS Publications website at DOI: 10.1021/jacs.6b07968.

> Experimental and characterization details, including NMR spectroscopic data, X-ray and neutron crystallographic data, and computational details (PDF)
> Coordinates, Input Files and Movies (gif) for the computational studies (ZIP)
> CIF data for the structures (X-ray and neutron) reported (CIF)

■ AUTHOR INFORMATION

Corresponding Authors
*S.A.Macgregor@hw.ac.uk
*andrew.weller@chem.ox.ac.uk

Author Contributions
[⊥]F.M.C. and T.K. contributed equally.

Notes
The authors declare no competing financial interest. Crystallographic data have been deposited with the Cambridge Crystallographic Data Center (CCDC) and can be obtained via www.ccdc.cam.ac.uk/data_request/cif (CCDC 1495160-4).

■ REFERENCES

(1) Alkane C-H Activation by Single-Site Metal Catalysis. Perez, P. J., Ed.; *Catal. Met. Complexes* **2012**, Vol. 38.
(2) Cavaliere, V. N.; Mindiola, D. J. *Chem. Sci.* **2012**, 3, 3356.
(3) Cook, A. K.; Schimler, S. D.; Matzger, A. J.; Sanford, M. S. *Science* **2016**, 351, 1421.
(4) Bergman, R. G. *Nature* **2007**, 446, 391.
(5) Activation and Functionalization of C−H Bonds. Goldberg, K. I., Goldman, A. S., Eds.; *ACS Syp. Ser.* **2004**; Vol. 885.
(6) Crabtree, R. H. *J. Organomet. Chem.* **2004**, 689, 4083.
(7) A special issue of *Chemical Reviews* is dedicted to C−H activation. See Crabtree, R. H. *Chem. Rev.* **2010**, 110, 575.
(8) Choi, J.; MacArthur, A. H. R.; Brookhart, M.; Goldman, A. S. *Chem. Rev.* **2011**, 111, 1761.
(9) Kumar, A.; Zhou, T.; Emge, T. J.; Mironov, O.; Saxton, R. J.; Krogh-Jespersen, K.; Goldman, A. S. *J. Am. Chem. Soc.* **2015**, 137, 9894.
(10) Ahuja, R.; Punji, B.; Findlater, M.; Supplee, C.; Schinski, W.; Brookhart, M.; Goldman, A. S. *Nat. Chem.* **2011**, 3, 167.
(11) Haibach, M. C.; Kundu, S.; Brookhart, M.; Goldman, A. S. *Acc. Chem. Res.* **2012**, 45, 947.
(12) Leitch, D. C.; Lam, Y. C.; Labinger, J. A.; Bercaw, J. E. *J. Am. Chem. Soc.* **2013**, 135, 10302.
(13) Sadow, A. D.; Tilley, T. D. *J. Am. Chem. Soc.* **2003**, 125, 7971.
(14) Goldman, A. S.; Roy, A. H.; Huang, Z.; Ahuja, R.; Schinski, W.; Brookhart, M. *Science* **2006**, 312, 257.
(15) Chen, H.; Schlecht, S.; Semple, T. C.; Hartwig, J. F. *Science* **2000**, 287, 1995.
(16) Jia, X.; Huang, Z. *Nat. Chem.* **2016**, 8, 157.
(17) Caballero, A.; Despagnet-Ayoub, E.; Mar Díaz-Requejo, M.; Díaz-Rodríguez, A.; González-Núñez, M. E.; Mello, R.; Muñoz, B. K.; Ojo, W.-S.; Asensio, G.; Etienne, M.; Pérez, P. J. *Science* **2011**, 332, 835.
(18) Chen, K.; Que, L. *J. Am. Chem. Soc.* **2001**, 123, 6327.
(19) Hall, C.; Perutz, R. N. *Chem. Rev.* **1996**, 96, 3125.
(20) Perutz, R. N.; Sabo-Etienne, S. *Angew. Chem., Int. Ed.* **2007**, 46, 2578.
(21) Lersch, M.; Tilset, M. *Chem. Rev.* **2005**, 105, 2471.
(22) Jones, W. D. *Inorg. Chem.* **2005**, 44, 4475.
(23) Chen, G. S.; Labinger, J. A.; Bercaw, J. E. *Proc. Natl. Acad. Sci. U. S. A.* **2007**, 104, 6915.
(24) Pitts, A. L.; Wriglesworth, A.; Sun, X.-Z.; Calladine, J. A.; Zaric, S. D.; George, M. W.; Hall, M. B. *J. Am. Chem. Soc.* **2014**, 136, 8614.
(25) Cobar, E. A.; Khaliullin, R. Z.; Bergman, R. G.; Head-Gordon, M. *Proc. Natl. Acad. Sci. U. S. A.* **2007**, 104, 6963.

(26) Bernskoetter, W. H.; Schauer, C. K.; Goldberg, K. I.; Brookhart, M. *Science* **2009**, *326*, 553.

(27) Calladine, J. A.; Torres, O.; Anstey, M.; Ball, G. E.; Bergman, R. G.; Curley, J.; Duckett, S. B.; George, M. W.; Gilson, A. I.; Lawes, D. J.; Perutz, R. N.; Sun, X.-Z.; Vollhardt, K. P. C. *Chem. Sci.* **2010**, *1*, 622.

(28) Yau, H. M.; McKay, A. I.; Hesse, H.; Xu, R.; He, M.; Holt, C. E.; Ball, G. E. *J. Am. Chem. Soc.* **2016**, *138*, 281.

(29) Cowan, A. J.; George, M. W. *Coord. Chem. Rev.* **2008**, *252*, 2504.

(30) Torres, O.; Calladine, J. A.; Duckett, S. B.; George, M. W.; Perutz, R. N. *Chem. Sci.* **2015**, *6*, 418.

(31) Evans, D. R.; Drovetskaya, T.; Bau, R.; Reed, C. A.; Boyd, P. D. *J. Am. Chem. Soc.* **1997**, *119*, 3633.

(32) Castro-Rodriguez, I.; Nakai, H.; Gantzel, P.; Zakharov, L. N.; Rheingold, A. L.; Meyer, K. *J. Am. Chem. Soc.* **2003**, *125*, 15734.

(33) Andreychuk, N. R.; Emslie, D. J. H. *Angew. Chem.* **2013**, *125*, 1740.

(34) Ball, G. E.; Brookes, C. M.; Cowan, A. J.; Darwish, T. A.; George, M. W.; Kawanami, H. K.; Portius, P.; Rourke, J. P. *Proc. Natl. Acad. Sci. U. S. A.* **2007**, *104*, 6927.

(35) Bernskoetter, W. H.; Hanson, S. K.; Buzak, S. K.; Davis, Z.; White, P. S.; Swartz, R.; Goldberg, K. I.; Brookhart, M. J. *J. Am. Chem. Soc.* **2009**, *131*, 8603.

(36) Gross, C. L.; Girolami, G. S. *J. Am. Chem. Soc.* **1998**, *120*, 6605.

(37) Sawyer, K. R.; Cahoon, J. F.; Shanoski, J. E.; Glascoe, E. A.; Kling, M. F.; Schlegel, J. P.; Zoerb, M. C.; Hapke, M.; Hartwig, J. F.; Webster, C. E.; Harris, C. B. *J. Am. Chem. Soc.* **2010**, *132*, 1848.

(38) Asplund, M. C.; Snee, P. T.; Yeston, J. S.; Wilkens, M. J.; Payne, C. K.; Yang, H.; Kotz, K. T.; Frei, H.; Bergman, R. G.; Harris, C. B. *J. Am. Chem. Soc.* **2002**, *124*, 10605.

(39) Cowan, A. J.; Portius, P.; Kawanami, H. K.; Jina, O. S.; Grills, D. C.; Sun, X. Z.; McMaster, J.; George, M. W. *Proc. Natl. Acad. Sci. U. S. A.* **2007**, *104*, 6933.

(40) Hartwig, J. F. *Organotransition Metal Chemistry*; University Science Books: Sausalito, USA, 2010.

(41) Alcaraz, G.; Sabo-Etienne, S. *Coord. Chem. Rev.* **2008**, *252*, 2395.

(42) Jones, W. D. *Acc. Chem. Res.* **2003**, *36*, 140.

(43) Pike, S. D.; Weller, A. S. *Philos. Trans. R. Soc., A* **2015**, *373*, 20140187.

(44) Huang, Z.; White, P. S.; Brookhart, M. *Nature* **2010**, *465*, 598.

(45) Van Der Boom, M. E. *Angew. Chem., Int. Ed.* **2011**, *50*, 11846.

(46) Coville, N. J.; Cheng, L. *J. Organomet. Chem.* **1998**, *571*, 149.

(47) Pike, S. D.; Thompson, A. L.; Algarra, A. G.; Apperley, D. C.; Macgregor, S. A.; Weller, A. S. *Science* **2012**, *337*, 1648.

(48) Pike, S. D.; Chadwick, F. M.; Rees, N. H.; Scott, M. P.; Weller, A. S.; Krämer, T.; Macgregor, S. A. *J. Am. Chem. Soc.* **2015**, *137*, 820.

(49) Chadwick, F. M.; Rees, N. H.; Weller, A. S.; Krämer, T.; Iannuzzi, M.; Macgregor, S. A. *Angew. Chem., Int. Ed.* **2016**, *55*, 3677.

(50) Inokuma, Y.; Kawano, M.; Fujita, M. *Nat. Chem.* **2011**, *3*, 349.

(51) Petrosko, S. H.; Johnson, R.; White, H.; Mirkin, C. A. *J. Am. Chem. Soc.* **2016**, *138*, 7443.

(52) Walter, M. D.; White, P. S.; Schauer, C. K.; Brookhart, M. *J. Am. Chem. Soc.* **2013**, *135*, 15933.

(53) Nguyen, B.; Brown, J. M. *Adv. Synth. Catal.* **2009**, *351*, 1333.

(54) Schrock, R. R.; Osborn, J. A. *J. Am. Chem. Soc.* **1976**, *98*, 4450.

(55) Edwards, A. J. *Aust. J. Chem.* **2011**, *64*, 869.

(56) Wilson, C. C. *Single Crystal Neutron Diffraction From Molecular Materials*; World Scientific Pub Co Inc: Singapore, 2000; Vol. 2.

(57) Douglas, T. M.; Weller, A. S. *New J. Chem.* **2008**, *32*, 966.

(58) Bianchini, C.; Frediani, P.; Graziani, M.; Kaspar, J.; Meli, A.; Peruzzini, M.; Vizza, F. *Organometallics* **1993**, *12*, 2886.

(59) Siedle, A. R.; Newmark, R. A. *J. Am. Chem. Soc.* **1989**, *111*, 2058.

(60) Siedle, A.; Newmark, R.; Sahyun, M.; Lyon, P.; Hunt, S.; Skarjune, R. *J. Am. Chem. Soc.* **1989**, *111*, 8346.

(61) Siedle, A.; Newmark, R.; Brown-Wensley, K.; Skarjune, R.; Haddad, L.; Hodgson, K.; Roe, A. *Organometallics* **1988**, *7*, 2078.

(62) Pike, S. D.; Krämer, T.; Rees, N. H.; Macgregor, S. A.; Weller, A. S. *Organometallics* **2015**, *34*, 1487.

(63) Kubas, G. J. *Metal Dihydrogen and σ-Bond Complexes*; Kluwer: New York, 2001.

(64) Hebden, T. J.; Denney, M. C.; Pons, V.; Piccoli, P. M. B.; Koetzle, T. F.; Schultz, A. J.; Kaminsky, W.; Goldberg, K. I.; Heinekey, D. M. *J. Am. Chem. Soc.* **2008**, *130*, 10812.

(65) Tang, C. Y.; Phillips, N.; Bates, J. I.; Thompson, A. L.; Gutmann, M. J.; Aldridge, S. *Chem. Commun.* **2012**, *48*, 8096.

(66) Smart, K. A.; Grellier, M.; Coppel, Y.; Vendier, L.; Mason, S. A.; Capelli, S. C.; Albinati, A.; Montiel-Palma, V.; Munoz-Hernandez, M. A.; Sabo-Etienne, S. *Inorg. Chem.* **2014**, *53*, 1156.

(67) Grellier, M.; Mason, S. A.; Albinati, A.; Capelli, S. C.; Rizzato, S.; Bijani, C.; Coppel, Y.; Sabo-Etienne, S. *Inorg. Chem.* **2013**, *52*, 7329.

(68) Bloch, E. D.; Queen, W. L.; Krishna, R.; Zadrozny, J. M.; Brown, C. M.; Long, J. R. *Science* **2012**, *335*, 1606.

(69) Geier, S. J.; Mason, J. A.; Bloch, E. D.; Queen, W. L.; Hudson, M. R.; Brown, C. M.; Long, J. R. *Chem. Sci.* **2013**, *4*, 2054.

(70) Hulvey, Z.; Vlaisavljevich, B.; Mason, J. A.; Tsivion, E.; Dougherty, T. P.; Bloch, E. D.; Head-Gordon, M.; Smit, B.; Long, J. R.; Brown, C. M. *J. Am. Chem. Soc.* **2015**, *137*, 10816.

(71) The other ~5% of the NBA is assigned to an isomer in which D_2 had added with *exo*-selectivity (see the Supporting Information). We assign this to the *endo*-D_2-*exo*-D_2-NBA isomer.

(72) Budzelaar, P. H.; Moonen, N. N.; de Gelder, R.; Smits, J. M.; Gal, A. W. *Eur. J. Inorg. Chem.* **2000**, *2000*, 753.

(73) Vitórica-Yrezábal, I. J.; Mínguez Espallargas, G.; Soleimannejad, J.; Florence, A. J.; Fletcher, A. J.; Brammer, L. *Chem. Sci.* **2013**, *4*, 696.

(74) Zenkina, O. V.; Keske, E. C.; Wang, R.; Crudden, C. M. *Angew. Chem., Int. Ed.* **2011**, *50*, 8100.

(75) Chierotti, M. R.; Gobetto, R. *Eur. J. Inorg. Chem.* **2009**, *2009*, 2581.

(76) Edwards, A. J.; Burke, N. J.; Dobson, C. M.; Prout, K.; Heyes, S. J. *J. Am. Chem. Soc.* **1995**, *117*, 4637.

(77) Chaplin, A. B.; Green, J. C.; Weller, A. S. *J. Am. Chem. Soc.* **2011**, *133*, 13162.

(78) Silvernail, N. J.; Barabanschikov, A.; Sage, J. T.; Noll, B. C.; Scheidt, W. R. *J. Am. Chem. Soc.* **2009**, *131*, 2131.

(79) Gutmann, T.; Walaszek, B.; Yeping, X.; Waechtler, M.; del Rosal, I.; Gruenberg, A.; Poteau, R.; Axet, R.; Lavigne, G.; Chaudret, B. *J. Am. Chem. Soc.* **2010**, *132*, 11759.

(80) Walaszek, B.; Adamczyk, A.; Pery, T.; Yeping, X.; Gutmann, T.; Amadeu, N. d. S.; Ulrich, S.; Breitzke, H.; Vieth, H. M.; Sabo-Etienne, S.; Chaudret, B.; Limbach, H.-H.; Buntkowsky, G. *J. Am. Chem. Soc.* **2008**, *130*, 17502.

(81) *NMR Crystallography*; Harris, R. K., Wasylishen, R. E., Duer, M. J., Eds.; John Wiley & Sons: Chichester, 2009.

(82) Gutmann, T.; del Rosal, I.; Chaudret, B.; Poteau, R.; Limbach, H.-H.; Buntkowsky, G. *ChemPhysChem* **2013**, *14*, 3026.

(83) Periana, R. A.; Bergman, R. G. *J. Am. Chem. Soc.* **1986**, *108*, 7346.

(84) Lawes, D. J.; Darwish, T. A.; Clark, T.; Harper, J. B.; Ball, G. E. *Angew. Chem., Int. Ed.* **2006**, *45*, 4486.

(85) Kubas, G. J.; Unkefer, C. J.; Swanson, B. I.; Fukushima, E. *J. Am. Chem. Soc.* **1986**, *108*, 7000.

(86) Carr, N.; Dunne, B. J.; Mole, L.; Orpen, A. G.; Spencer, J. L. *J. Chem. Soc., Dalton Trans.* **1991**, 863.